Supplement of Hydrol. Earth Syst. Sci., 29, 7127–7147, 2025
https://doi.org/10.5194/hess-29-7127-2025-supplement

Hydrology and Earth System Sciences
Open Access

Supplement of

Field-scale modelling reveals dynamic groundwater flow and transport patterns in a high-energy subterranean estuary

Janek Greskowiak et al.

Correspondence to: Janek Greskowiak (janek.greskowiak@uni-oldenburg.de)

Section S1: Governing equations in SEAWAT

$$\nabla \cdot \left(\rho K_f \left[\nabla h_f + \frac{\rho - \rho_f}{\rho_f} \nabla z \right] \right) = \rho S_f \frac{\partial h_f}{\partial t} + \theta \frac{\partial \rho}{\partial C} \frac{\partial C}{\partial t} - \rho_s q_s \qquad \text{(Eq. S1)}$$

$$\frac{\partial (\theta C)}{\partial t} = \nabla \cdot \left(\theta D \nabla C \right) - \nabla \theta v C - q_s C_s \qquad \text{(Eq. S2)}$$

with

$$\rho = 0.714 \cdot C + \rho_f \qquad \text{(Eq. S 3)}$$

where ρ = fluid density (ML^{-3}), K_f = equivalent fresh water hydraulic conductivity tensor (LT^{-1}), h_f = equivalent fresh water head (L), z = elevation (L), S_f = equivalent fresh water specific storage (L^{-1}), t = time (T), θ = porosity (dimensionless), C = dissolved salt concentration (ML^{-3}), ρ_s = fluid density in source/sink, q_s = source/sink flow rate (T^{-1}), D = hydrodynamic dispersion tensor ($L^2\ T^{-1}$), v = pore water velocity (L/T), C_s = salt concentration in sources/sinks.

Section S2: Model domain

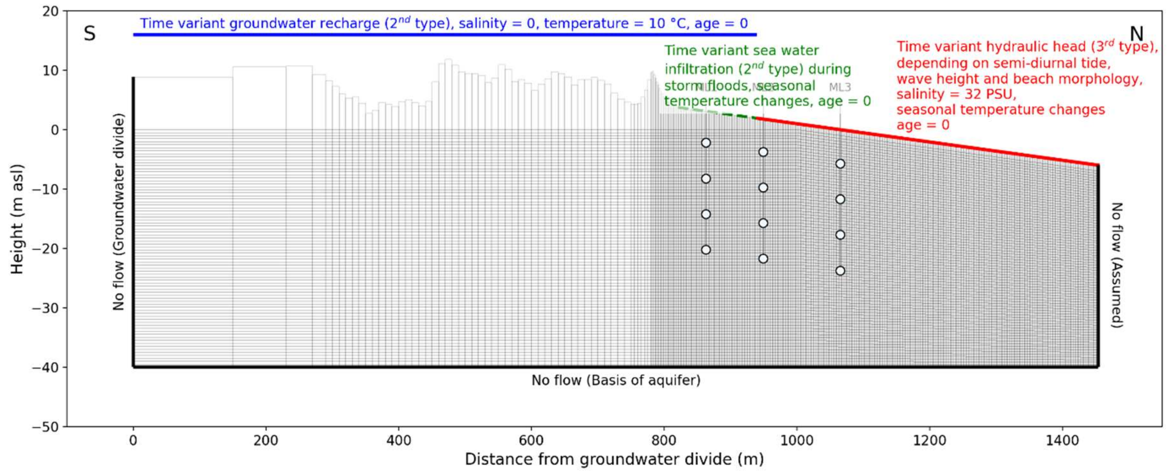

Figure S1: Model domain and defined boundary conditions. The multi-level observation wells ML1, ML2 and ML3 are presented for a better orientation.

Section S3: Hydraulic heads

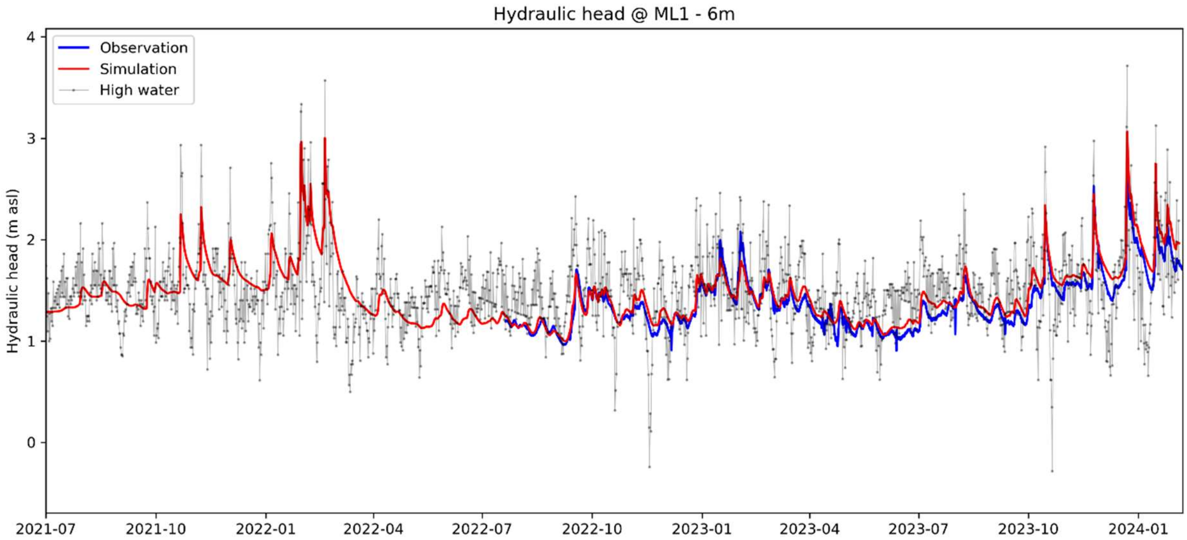

Figure S2: Simulated (red) and observed (blue) hydraulic heads at ML1-6m, and high water level (black) as sum of high tide and wave setup.

Section S4: Calculation of the monthly groundwater recharge

Groundwater recharge information for Spiekeroog Island was available from the regional water balance model mGROWA22 (Hajati et al., 2022) only until 2020, which calculated an annual recharge of 400-450 mm/a for the area upstream (i.e. south) of the investigated field site. In order to cover the entire simulation period, especially the period where detailed field data exists (July 2022 - February 2024), available monthly climatic water balance data from the nearby barrier island Norderney (30 km west of Spiekeroog) provided by the German Weather Service (DWD) was used in conjunction with the mGROWA22 estimated average groundwater recharge. For that the following assumptions were made: (i) For a negative climatic water balance (i.e., precipitation is less than potential evapotranspiration), no loss of groundwater due to evapotranspiration occurred and the monthly groundwater recharge was set to zero. This is justified as the mGROWA-calculated loss related to evapotranspiration during the summer was less than 2% of the total annual groundwater recharge. (ii) if positive, the climatic water balance on Norderney, scaled by the mGROWA-based average annual recharge of 425 mm/a on Spiekeroog, reflects the monthly groundwater recharge on Spiekeroog.

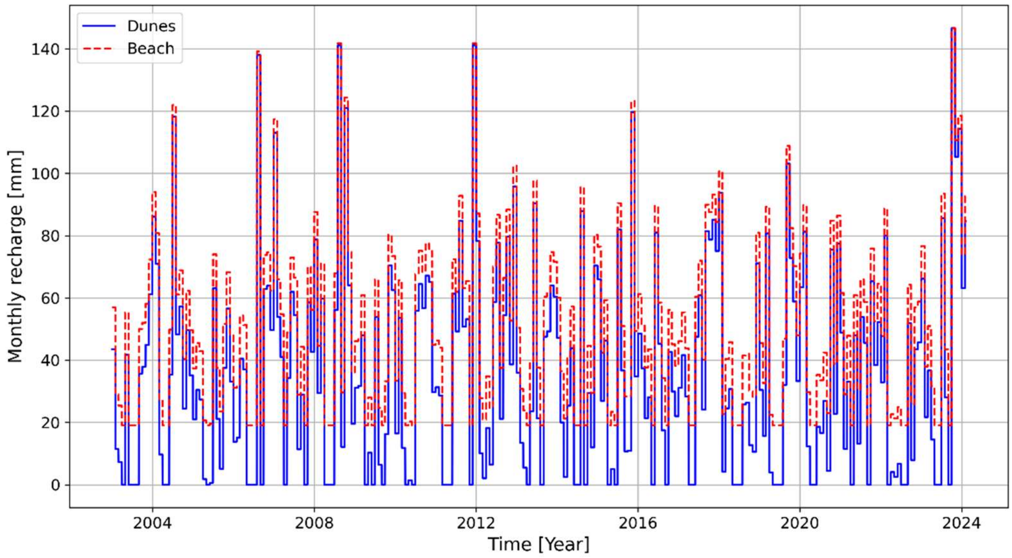

Figure S3: Applied monthly groundwater recharge in dune and beach areas.

Section S5: Time series of high and low water levels

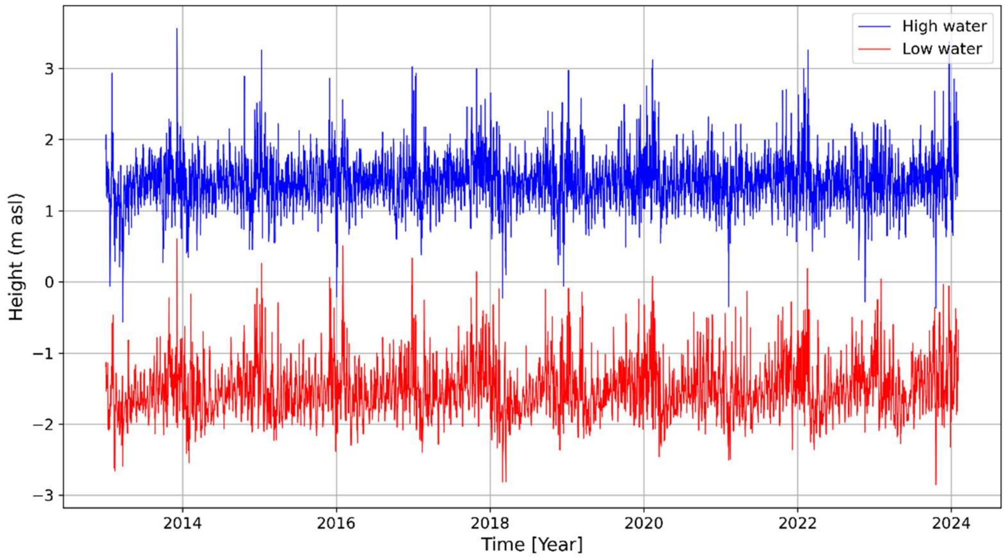

Figure S4: High and low tide level from employed tide time series.

Section S6: Time series of significant wave height

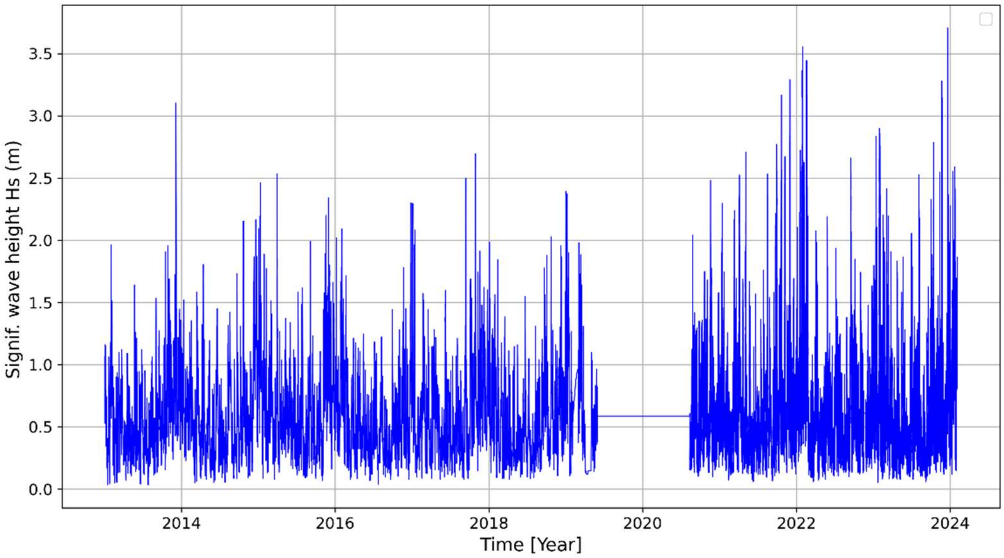

Figure S5: Employed significant wave height for the calculation of the wave set up. Missing data were filled with the mean significant wave height.

Section S7: Calculation of tide-averaged hydraulic heads at the seaside boundary condition

The applied hydraulic head at the seaside boundary was a function of local topographic height, tidal signal and significant wave height, based on the tide-averaging approach of Nuttle (1991). In this approach it is assumed that a location on the aquifer-sea boundary below the high tide mark receives a hydraulic head equal to the topographic height if the tide is lower than the topography at this position. Hence it is assumed that the time to drain the aquifer is not sufficient to significantly lower the groundwater level during ebbing tide. Or in other words, seepage is assumed everywhere along the un-inundated beach face between high water mark and actual sea level position. If the actual tide elevation is higher than the respective location, the hydraulic head is equal to the tidal elevation. Averaging the hydraulic head over time for each position over a tidal period results in a curve that declines from the topographic elevation at the high tide mark to zero at the low tide mark and beyond. The approach of Nuttle (1991) was extended by adding the wave setup using an empirical formulation by Nielsen (2009):

$$\eta = \frac{0.4H_{RMS}}{1+10\dfrac{D+\eta}{H_{RMS}}} \qquad \text{(Eq. S 4)}$$

where η is the phase-averaged increase above the still water level (i.e., the actual seawater level without waves) depending on root-mean-square wave height H_{RMS} and still water depth D. The root-mean-square wave height H_{RMS} can be calculated from the significant wave height H_{sig} as $H_{RMS} = 0.5\sqrt{2}H_{sig}$ (Holthuijsen, 2007).

For each minute data the actual hydraulic head was calculated from tide-level and wave setup at a given position, and then averaged over time for a whole tidal cycle by Nuttle's approach.

Section S8: Time series of beach topography

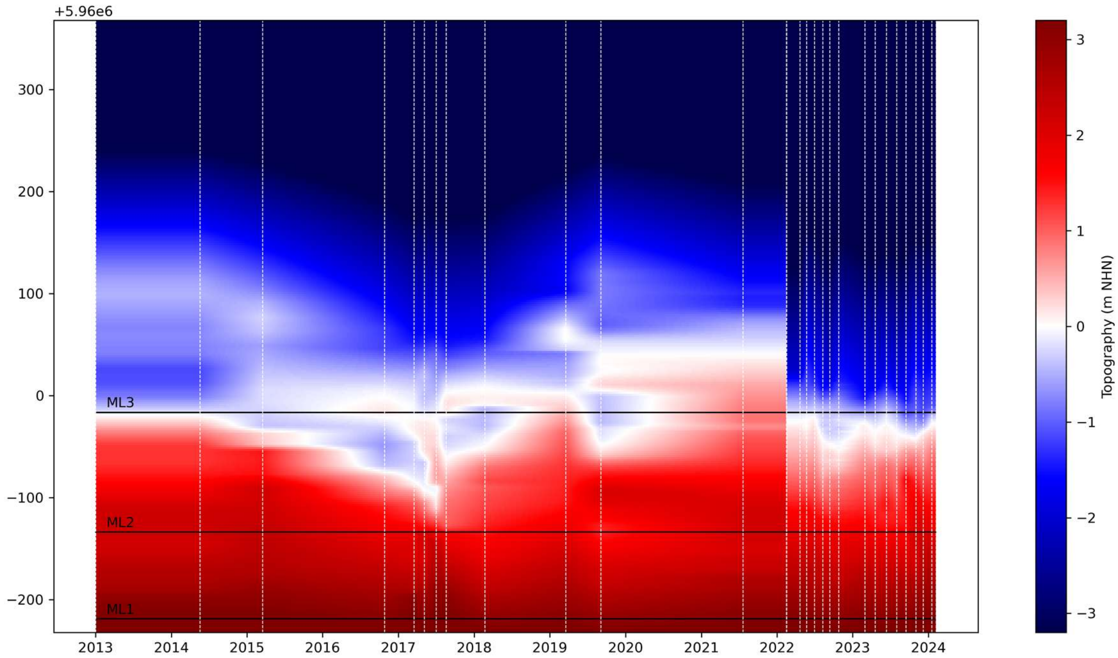

Figure S6: Evolution of beach topography with time. Vertical dashed lines indicate time points of measurements. The y-axis is given in UTM32-North.

Section S9: Observation weights used during the optimization

The PSO algorithm minimizes the following objective function ϕ:

$$\Phi = \sum_{i=1}^{N} \left(w_i (obs_i - sim_i) \right)^2 \qquad \text{Eq. S5)}$$

Where N is the total number of data points, obs_i, and sim_i are the observed and simulated data point i and w_i the associated weight of this data point in the objective function.

In this work, G = 5 observation groups k, namely (1) hydraulic heads, (2) salinity, (3) temperature at the multi-level monitoring wells and (4) temperature at SAMOS and (5) groundwater ages were treated separately in the objective function, by assigning group-specific weights w_k (Table S1), i.e., a constant weight for all data points in an observation group k:

$$\Phi = \sum_{k=1}^{G} \sum_{i=1}^{N_k} \left(w_k (obs_i - sim_i) \right)^2 \qquad \text{(Eq. S6)}$$

Where N_k is the total number of observation points observation group k.

Table S1: Observation group specific weights

Observation group	**Weight**
Hydraulic heads	0.029 m^{-1}
Salinity	0.056 PSU^{-1}
Temperature at ML1,2, and 3	0.010 $°C^{-1}$

Temperature at SAMOS	0.012 °C^{-1}
Groundwater age	0.139 a^{-1}

Section S10: Convergence of the PSO optimization

The preliminary optimization runs for finding optimal weights and an optimal number of pilot points by trial- and error indicated that 100 iterations were sufficient to converge to the global minimum (Figure S7). Though, more iterations than that could further bring down the objective function to some little extent, but virtually led to no visual improvement of the model fit.

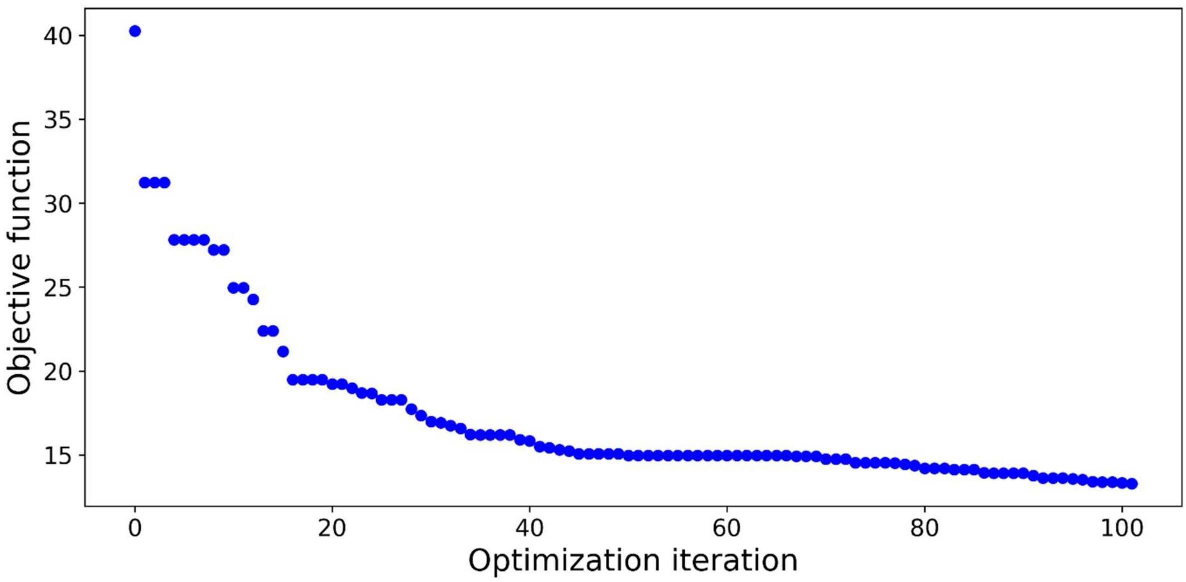

Figure S7: Objective function over the course of the optimization.

At the end of the optimisation run it is noticeable that for some parameters the spreading of the particles (i.e., parameter values associated with the particles) is broader than for others (Figure S8), suggesting their lower sensitivity on model results. A rigorous parameter sensitivity assessment, however, is not possible with the PSO approach.

Note that due to computational constrains of the High Performance Computer, the optimization was split in two subsequent batches of 50 iterations each. The second batch uses initial parameter values that came out at the end of the first batch as best particle values, but with re-set inertia of the particle velocities. This gives some perturbation at the beginning of the second batch, i.e., at optimization iteration 50 (Figure S8). While this leads to some delay in the convergence (Figure S7), it is still beneficial for further overcoming undesired local minima in the objective function.

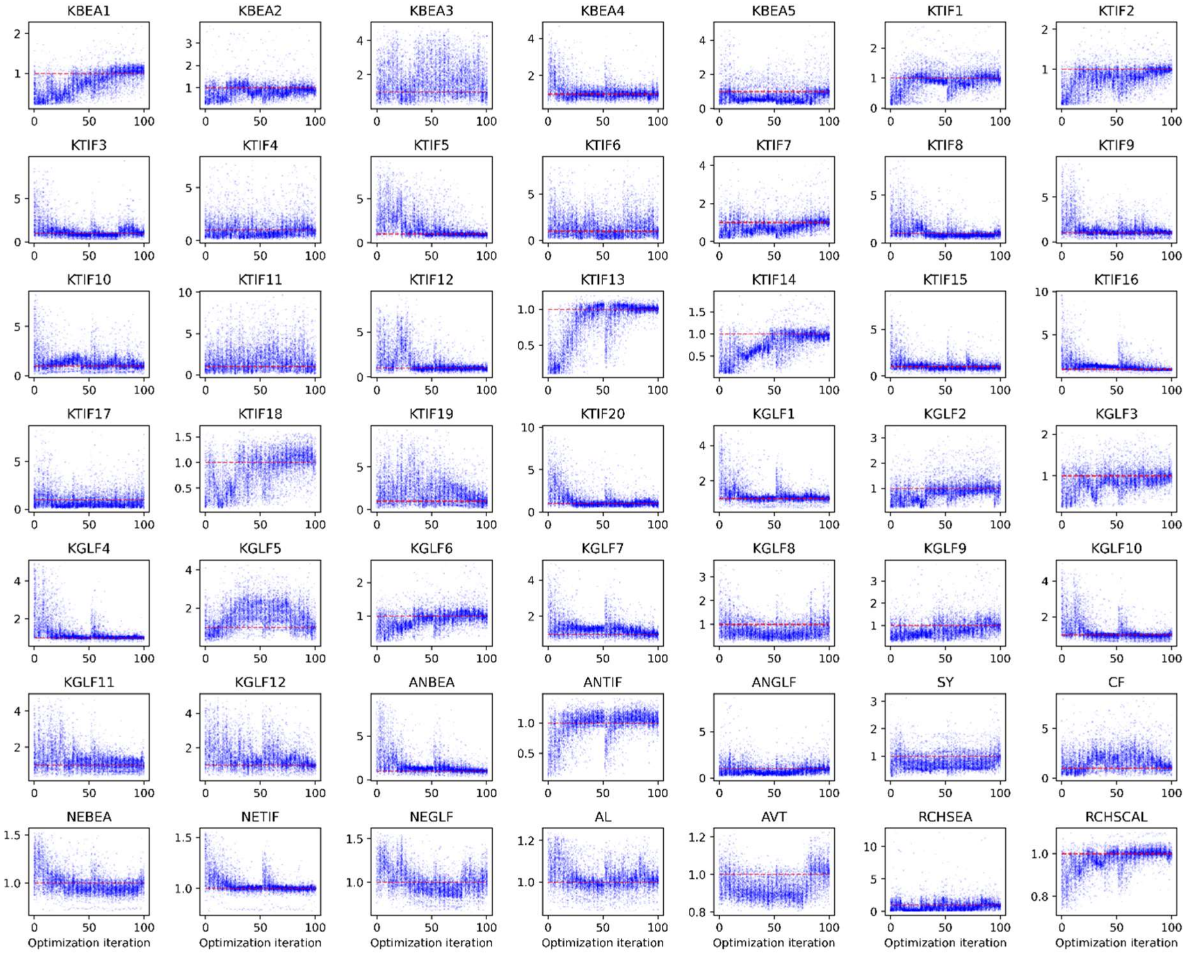

Figure S8: Evolution of the particle swarm (100 particles) for each parameter (normalized to the final value) over 100 optimization iterations (little blue dots). The dashed red line indicates the final normalized parameter value.

Section S11: Scatter diagrams and calibration performance measures

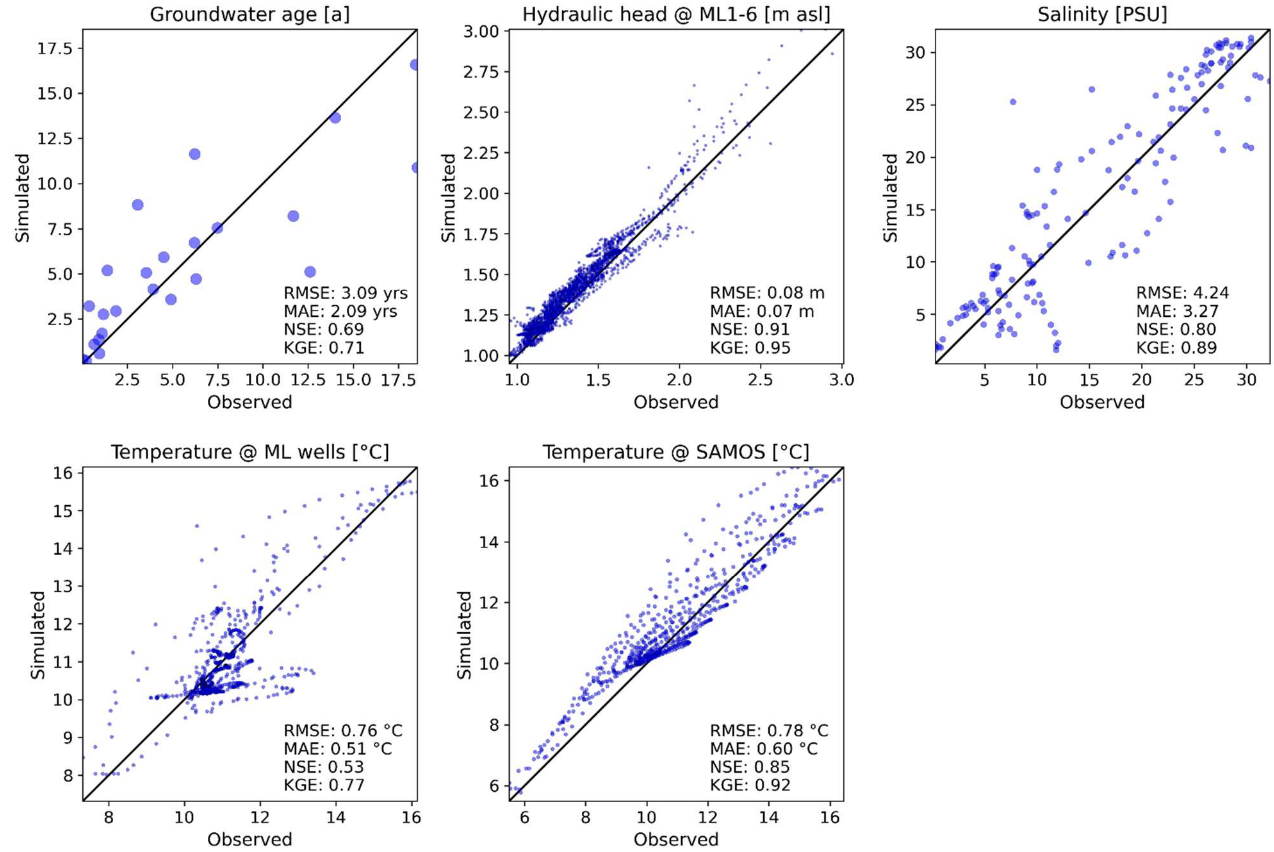

Figure S9: Scatter diagrams of simulated versus observed state variables, and their respective calibration performance measures root mean square error (RMSE), mean absolute error (MAE), Nash-Sutcliff Efficiency (NSE) and Kling-Gupta Efficiency (KGE) for the final calibrated model. The performance measures were calculated for each individual observation groups by using the unweighted residuals between simulation and observation.

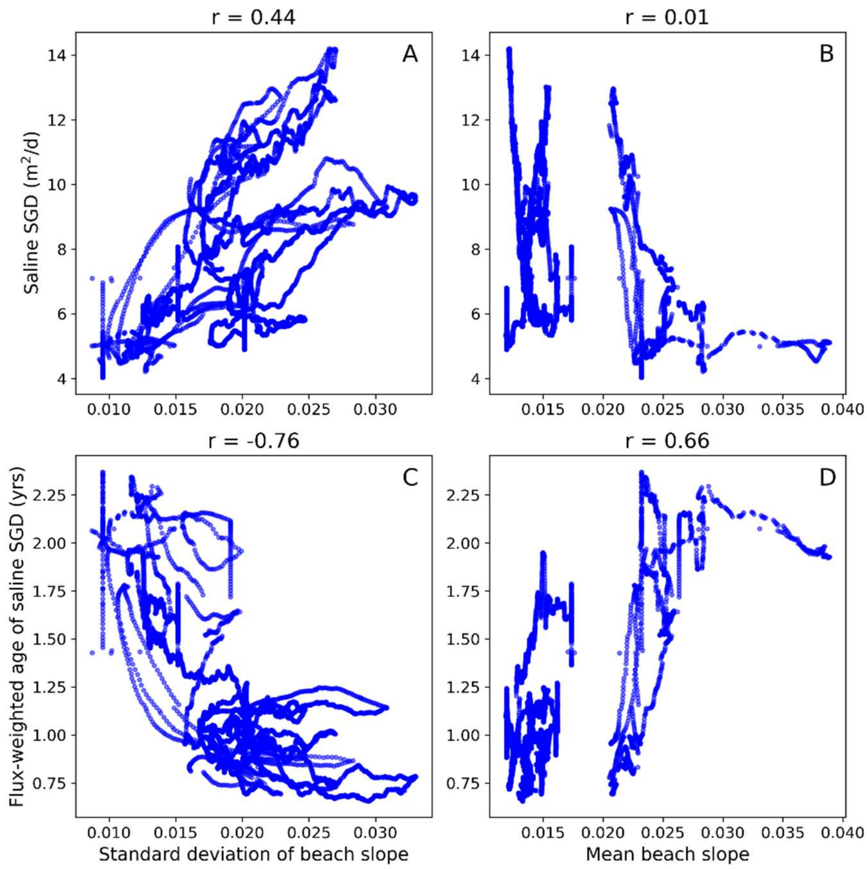

Figure S10: Scatter diagrams of simulated saline SGD versus (A) the standard deviation of beach slope and (B) the mean beach slope, and its flux weighted age versus (C) the standard deviation of beach slope and (D) the mean beach slope, with the corresponding Pearson correlation coefficient r.

Section S12: Video Animation

Video S1: Animation that shows simulated Salinity, groundwater age and temperature along the modelled cross-section at the study site between July, 2016 and February, 2024.

References

Holthuijsen, L.H., 2007. Waves in Oceanic and Coastal Waters. Cambridge University Press, Cambridge. https://doi.org/10.1017/CBO9780511618536

Nuttle, W.K., 1991. Comment on "Tidal dynamics of the water table in beaches" by Peter Nielsen. Water Resources Research 27, 1781–1782. https://doi.org/10.1029/91WR00939